Investigation of land ice-ocean interaction with a fully coupled ice-ocean model: 1. Model description and behavior

D. N. Goldberg,[1] C. M. Little,[2] O. V. Sergienko,[3] A. Gnanadesikan,[4] R. Hallberg,[5] and M. Oppenheimer[2]

Received 11 October 2011; revised 11 May 2012; accepted 18 May 2012; published 29 June 2012.

[1] Antarctic ice shelves interact closely with the ocean cavities beneath them, with ice shelf geometry influencing ocean cavity circulation, and heat from the ocean driving changes in the ice shelves, as well as the grounded ice streams that feed them. We present a new coupled model of an ice stream-ice shelf-ocean system that is used to study this interaction. The model is capable of representing a moving grounding line and dynamically responding ocean circulation within the ice shelf cavity. Idealized experiments designed to investigate the response of the coupled system to instantaneous increases in ocean temperature show ice-ocean system responses on multiple timescales. Melt rates and ice shelf basal slopes near the grounding line adjust in 1–2 years, and downstream advection of the resulting ice shelf thinning takes place on decadal timescales. Retreat of the grounding line and adjustment of grounded ice takes place on a much longer timescale, and the system takes several centuries to reach a new steady state. During this slow retreat, and in the absence of either an upward-or downward-sloping bed or long-term trends in ocean heat content, the ice shelf and melt rates maintain a characteristic pattern relative to the grounding line.

Citation: Goldberg, D. N., C. M. Little, O. V. Sergienko, A. Gnanadesikan, R. Hallberg, and M. Oppenheimer (2012), Investigation of land ice-ocean interaction with a fully coupled ice-ocean model: 1. Model description and behavior, *J. Geophys. Res.*, *117*, F02037, doi:10.1029/2011JF002246.

1. Introduction

[2] The large ice shelves bordering the Antarctic coastline play an important role in both the hydrography of the Southern Ocean and the mass balance and configuration of the Antarctic Ice Sheet. On the oceanographic side, ice shelves provide a surface boundary condition that is different than either open ocean or sea ice, with water subject to a depth-dependent freezing point and relatively large gradients in surface hydrostatic pressure. The induced submarine melting and freezing and density-driven circulation affect nearby seawater properties [*Jacobs et al.*, 1970; *Jenkins*, 1999; *Nicholls et al.*, 2009].

[3] On the glaciological side, the ice shelves control the distribution of normal stresses at the grounding line, which in turn affects ice mass flux there. Numerical simulation has shown that this distribution can change instantaneously with the thickness and/or extent of the ice shelf [e.g., *Schmeltz et al.*, 2002], and while the immediate response in ice velocity only penetrates on the order of ten ice thicknesses into the ice sheet [*Hindmarsh*, 2006; *Schoof*, 2007a], a thinning signal can be carried inland on a decadal timescale via dynamic draw-down [*Payne et al.*, 2004]. Thus ice shelves provide a pathway for the heat content of the ocean to cause changes in continental ice sheets.

[4] In the last two decades, observations of the Amundsen Sea ice shelves and the ice streams that feed them have been consistent with this story. The observed mass loss from Pine Island (PIG) and Thwaites Glaciers was too large to be accounted for by changes in surface mass balance [*Shepherd et al.*, 2002; *Shepherd and Wingham*, 2007]. Acceleration and grounding line retreat were also observed on PIG [*Rignot et al.*, 2002]. At the same time, high levels of mass loss were seen in the ice shelves fed by these glaciers, and it was suggested that ocean melting was the driver for these changes [*Shepherd et al.*, 2004; *Payne et al.*, 2004]. Very warm waters have been observed under Pine Island Ice Shelf

[1]Department of Earth, Atmospheric and Planetary Sciences, MIT, Cambridge, Massachusetts, USA.
[2]Woodrow Wilson School of Public and International Affairs, Princeton University, Princeton, New Jersey, USA.
[3]Department of Atmospheric and Oceanic Sciences, Princeton University, Princeton, New Jersey, USA.
[4]Department of Earth and Planetary Sciences, Johns Hopkins University, Baltimore, Maryland, USA.
[5]Geophysical Fluid Dynamics Laboratory, NOAA, Princeton, New Jersey, USA.

Corresponding author: D. N. Goldberg, Department of Earth, Atmospheric and Planetary Sciences, MIT, 77 Massachusetts Ave., Cambridge, MA 02139, USA. (dgoldber@mit.edu)

0148-0227/12/2011JF002246

[*Jenkins et al.*, 2010; *Jacobs et al.*, 2011], potentially capable of melting large volumes of ice. While direct measurements of melt rates on these ice shelves are not available, oceanographic outflow measurements imply area-averaged under-shelf melt rates of 20–25 ma^{-1} under Pine Island Ice Shelf [*Jacobs et al.*, 2011] and modeling studies imply local melt rates that are much higher [*Payne et al.*, 2007; *Heimbach and Losch*, 2012].

[5] While it is for the most part accepted that submarine melting can elicit a grounded ice response, questions remain. For instance, what is the signature of response of the ice stream-ice shelf system to a change in large-scale ocean conditions (i.e., conditions far from the shelf), and to what extent can observed ice thickness and velocity changes be attributed to such a perturbation? How will warming of the Southern Ocean (and/or changes in heat flux from the Southern Ocean on to the Antarctic continental shelf) affect the ice streams that feed West Antarctic ice shelves? Are there important feedbacks in the coupled ice stream-ice shelf-ocean cavity system, either positive or negative, and how do external factors affect these feedbacks? What are the intrinsic timescales characterizing the different interactions and feedbacks?

[6] Understanding of the evolution of this coupled system and its response to external forcing requires a new generation of coupled ice-ocean models. These models should account for the mutual effects and responses of grounded ice and ocean circulation. The melt-driven changes in grounded ice and the ice geometry-driven effects on ocean circulation should be accounted for [*Little et al.*, 2007; *Joughin and Alley*, 2011]. Both horizontal dimensions should be resolved, allowing potentially important effects in both ice and ocean components, such as ice shelf buttressing and ocean boundary currents, to be simulated.

[7] Previous modeling studies have addressed different aspects of these needs. Many ocean modeling studies have investigated basal melting under a static ice shelf, i.e., ocean models in which the ice shelf thickness and grounding line remained fixed [e.g., *Jenkins*, 1991; *Grosfeld et al.*, 1997; *Jenkins and Holland*, 2002; *Holland et al.*, 2003; *Payne et al.*, 2007; *Little et al.*, 2008; *Holland et al.*, 2008]. Although a variety of different types of ocean models with differing levels of complexity have been employed, and have generated similar conclusions regarding certain quantities (such as area-integrated melt), three-dimensional ocean models suggest that horizontal circulation and vertical mixing are required to capture the strong horizontal gradients in melt patterns that arise [*Little et al.*, 2009].

[8] Other studies have examined the glaciological response to melting. *Grosfeld and Sandhager* [2004] used a three-dimensional coupled dynamic ice shelf-ocean cavity model, in which the grounding line remain fixed. *Walker and Holland* [2007] developed a flowline coupled ice shelf-ocean model (i.e., a model in which one horizontal coordinate is resolved). As opposed to the asynchronous approach of *Grosfeld and Sandhager* [2004], their model advanced the ice shelf at the same timestep as the ocean. Still, there were technical difficulties in representing flow near the grounding line, which was static. *Parizek and Walker* [2010] used an asynchronously coupled flowline ice-ocean model that allowed for grounding line migration. *Joughin et al.* [2010] employed a three-dimensional ice stream-ice shelf model with realistic topography and basal traction to examine the response of PIG to ocean melting. In that study the authors forced the ice shelf with a depth-dependent melt parameterization informed by ocean modeling. *Pollard and DeConto* [2009] used a parameterization dependent on both depth and embayment protection for under-shelf melt rates in their modeling study (their treatment differed from that of *Joughin et al.* [2010] in part because they were considering the entire Antarctic Ice Sheet rather than a single ice shelf). *Little et al.* [2012] developed a melt rate parameterization based on ice shelf basal slope rather than depth, and implemented it in a flowline ice stream-ice shelf model with a dynamic grounding line. *Determann et al.* [2012] used melt rate fields generated by an ocean model to force an ice sheet-ice shelf model capable of grounding line movement, but the effect of evolving ice thickness on melt rates was not considered.

[9] All of the studies mentioned above attempted to assess the interaction of ice and ocean, and deepened our understanding of the processes involved; yet all were missing at least one of the components specified above as necessary to simulate land ice-ocean interaction (e.g., dynamic ice shelf grounding line, evolving ocean model, resolved transverse features). In this study, a three-dimensional ocean model is coupled to a two-dimensional (plan view) dynamic ice shelf-ice stream model capable of resolving grounding line migration. In this paper we present results from a single coupled experiment with a small, strongly thermally forced stream-shelf system similar to those of the Amundsen Sea (the term "stream-shelf system" refers to the fact that internal stresses are continuous between grounded and floating ice, and that the grounding line is allowed to evolve). The experiment is designed to examine the adjustment of the coupled system subsequent to a step change in far-field ocean conditions. The influence of the ocean cavity adjustment and grounded ice response on one another are complex, but a clear separation of timescales is observed between the coupled ice shelf-ocean adjustment and the grounded ice evolution. This separation of timescales has implications for future coupled modeling studies, as well as for attributing changes in ice dynamics to changes in ocean temperatures.

[10] While our experimental setup may bear some resemblance to the actual PIG ice stream-ice shelf-ocean cavity system, we emphasize that this study is not intended as a direct simulation of an existing glacier, nor is the imposed step change in far-field forcing presented as a realistic mode of change of ocean conditions. Rather, it is an idealized experiment designed to learn about key processes and interactions in such a system. In *Goldberg et al.* [2012], multiple experiments that assess the overall sensitivity of the response to both far-field ocean conditions and inland and grounded ice parameters are carried out.

2. Numerical Model

2.1. Ice Model

[11] The ice component of the coupled model implements the depth-integrated Shallow Shelf Approximation (SSA) of *MacAyeal* [1989] for an ice stream-ice shelf system with a dynamic grounding line. In this approximation, horizontal velocities are considered to be depth-independent, and are related to ice thickness and to each other through a non-

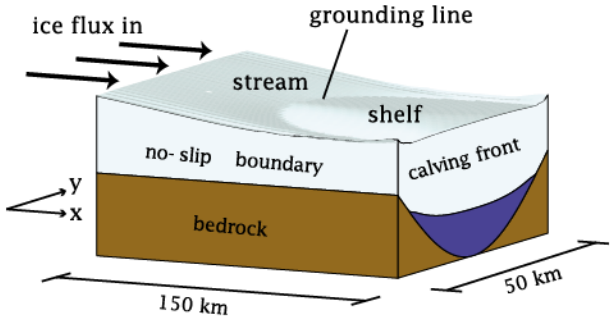

Figure 1. A representation of the ice model. The flow is predominantly in the x-direction. The bedrock elevation is independent of x; that is, the bed has the same cross-flow profile at all positions along the flow direction.

inertial, nonlinear, viscous stress balance with a Glen's law rheology [*Paterson*, 2001, chapter 5]. The ice is treated as isothermal (in the context of the flow law) and the Glen's law constant, i.e., the stiffness parameter, is constant.

[12] Under the SSA a simple floatation condition implicitly determines the position of the grounding line:

$$\rho_i h + \rho_w R(x,y) \begin{cases} \leq 0 & \text{for floating ice,} \\ > 0 & \text{for grounded ice.} \end{cases} \tag{1}$$

Here h is ice thickness (i.e., the difference in elevation between upper and lower surfaces), ρ_i is ice density, ρ_w is ocean density, and R is bedrock elevation (negative when below sea level). A single, representative value is used for ρ_w, rather than densities calculated by the ocean model (discussed below). Equation (1) allows the grounding line to evolve in time as a result of thickness change. A linear sliding law is used, of the form

$$\vec{\tau}_b = \beta^2 \vec{u}, \tag{2}$$

where $\vec{\tau}_b$ is basal stress and $\vec{u} = (u, v)$ is ice velocity in the x- and y-direction, respectively. β^2 is held spatially constant; however, basal stress is only present in the grounded domain, i.e., where the second case in equation (1) is met. While inertial terms are neglected in the momentum balance due to high viscosities, the ice evolves through the continuity equation with sources and sinks:

$$h_t = -h\nabla \cdot \vec{u} - \vec{u} \cdot \nabla h + a - \dot{m}, \tag{3}$$

where a is a surface accumulation term and $\dot{m}$ is a basal mass balance (positive where there is melting).

[13] The ice is modeled in a rectangular domain, 150 km long and 50 km wide (Figure 1). The boundary conditions are defined such that ice flow is predominantly along the longer axis. At the upstream boundary a depth-integrated flux, q_0, is imposed into the domain. This flux is represents transport of ice from the continental interior. The flux is constant along the upstream boundary, and is held constant in time in all experiments (as we are not investigating the effects of perturbations originating from the ice sheet interior).

[14] Along the sides of the domain there is assumed to be slow-moving ice capable of supporting substantial shear stress. This is represented by a no-flow boundary condition, i.e., $\vec{u} = 0$. At the downstream boundary a calving front is imposed. This implies a stress condition arising from the imbalance of depth-integrated pressure in the ice and in the ocean (*Weertman* [1957], modified for a calving cliff as in *Schoof* [2007b, Appendix B]). The ice flows over a nondeforming bed whose elevation R is given by the analytical expression

$$R(x,y) = -\left(300\,\text{m} + 600\,\text{m} \times \sin\left(\frac{\pi y}{L_y}\right)\right), \tag{4}$$

so that bed elevation does not vary in the principal direction of ice flow. The calving front is held fixed in all simulations, implying that all ice that crosses this boundary calves immediately. In all our experiments we set the surface accumulation a to a small, uniform value, but this input does not play a significant role in the mass balance. Of far greater importance is the basal melt rate $\dot{m}$, discussed in more detail below.

[15] This implementation of the upstream condition is somewhat nonstandard: velocity is set to zero, and the flux enters the domain through the continuity equation (3), which is implemented as a finite volume scheme. Such a condition is easier to implement in our model than Dirichlet conditions on both velocities and thickness, and can be seen as equivalent to having very strong accumulation in the first grid cell. As can be expected, within a few kilometers of this boundary there are high gradients in surface elevation and velocity, but this adjustment region is sufficiently far removed from the grounding line and any region of interest that it does not affect the solution.

[16] The ice model described here is essentially that of *Goldberg et al.* [2009] in a different configuration. That study established that the model is capable of robustly representing grounding line migration, as well as the junction between floating and grounded domains. Two kinds of mesh adaptation were discussed in the reference; in this study only h-refinement (selective refinement and coarsening of cells) is used, with variable resolution of either 1 km or 0.5 km.

2.2. Ocean Model

[17] The ocean component of the coupled model is the Hallberg Isopycnal Model [*Hallberg and Gnanadesikan*, 2006], modified for circulation under an ice shelf. The model allows for variable surface pressure to account for the influence of the weight of the ice shelf on the ocean pressure field, and it incorporates the three-equation parameterization of *Holland and Jenkins* [1999] for the thermodynamics of the viscous sublayer at the ice-ocean interface to calculate sub-shelf melt rates and heat and salt fluxes. The parameterization for basal melting requires a conductive heat flux into the ice. Since the ice model is isothermal, the steady state approximation for the ice shelf internal temperature from *Holland and Jenkins* [1999] is used for the basal vertical temperature gradient in the ice. This approach does not include horizontal heat advection within the ice shelf, but for high basal melting rates (as seen in the present study) it still may be a good approximation (see the discussion in section 5.3). The ocean model described here is essentially that of *Little et al.* [2009] in a different configuration.

[18] As previously done in studies of under-shelf ocean circulation, the profile of temperature and salinity is

Table 1. Physical Parameters Used in the Coupled Experiment[a]

Symbol	Constant	Value	Units
n	Glen's Law exponent	3	(none)
A	Glen's Law coefficient	3×10^{-25}	$Pa^{-3}\ s^{-1}$
β^2	sliding coefficient	9.6053×10^{8}	$Pa\ (m/s)^{-1}$
g	gravity	9.81	$m\ s^{-2}$
ρ_i	ice density	910	$kg\ m^{-3}$
ρ_w	ocean density[b]	1024	$kg\ m^{-3}$
τ_0	relaxation region strength at ocean boundary	50	day^{-1}
q_0	ice flux input	1.5×10^{6}	m^2/a
a	surface accumulation	0.3	ma^{-1}

[a]Note that β^2 corresponds to about 30 kPa where ice is moving 1 km/yr.
[b]This is the ocean density used by the ice model. The ocean model does not have uniform density.

maintained by restoring values within the ocean to a fixed profile in a region near the seaward boundary. Our restoring region is a 10 km-wide strip just seaward of the ice shelf front. The strength of the linear restoring (i.e., the inverse of the time constant) depends on distance from the ice shelf front as

$$\tau_{restore} = \tau_0 e^{\frac{x_f + 10 - x}{10}} \quad (5)$$

where τ_0 has units of inverse time, x is position in km, and x_f is the ice shelf front position. Aside from under-shelf melting (and possibly freezing) there is no surface forcing. All horizontal boundaries are no-flow conditions. The horizontal resolution is 1 km everywhere.

[19] The stratification specified in the restoring region represents far-field ocean conditions, and due to the small size of the domain it has a very strong influence on the ocean conditions under the ice shelf (the other influences being the buoyancy forcing due to melting, and the depth of the ice shelf base). The particular stratification used in this study is discussed below in section 2.4.

[20] Scalar parameters relevant to the ice and ocean model are found in Table 1.

2.3. Model Coupling

[21] In our coupled system, the ocean affects the ice solely through melting, while ice dynamics feed back on ocean circulation by changing the surface pressure and horizontal extent of the ocean. Note that, in addition to the dynamic effect of changing surface pressure, there is an implicit thermodynamic forcing on the ocean, since the parameterizations for freezing temperature and heat flux into the ice shelf depend on pressure and ice thickness, respectively.

[22] Given that we had a free-standing ocean code that could be run within any given ice cavity geometry and a free-standing ice code that could accept the melt rates produced by such a model, the simplest way to couple the models was to use the output from one to force the other in an asynchonous mode. The basal melt rate for a given geometry is calculated by the ocean model, which is then used to run the ice model to produce a new ice thickness field h. This geometry results in a hydrostatic ocean surface pressure at the ice shelf base given by $\rho_i g h$ which is then used to run the ocean model.

[23] The coupling is similar to that of *Grosfeld and Sandhager* [2004]; that is, the ocean is spun up from an initial state in each coupled timestep. At the beginning of each timestep, the ice shelf basal elevation and pressure is used to initialize the ocean model. Where $b - R < 10$ m (with b determined by the floatation depth of the ice shelf), the ocean depth is set to zero. The initial ocean state can be described as follows: there is a mixed layer with a uniform thickness of 10 m and a uniform temperature and salinity equal to their corresponding values in the restoring region. Below the mixed layer the initial interfaces of the isopycnals are flat, with each isopycnal layer having the same temperature, salinity, and thickness as in the restoring region, shown heuristically in Figure 2. The ocean model is integrated for a period of 15 days, and the average of the melt field over the final 5 days is passed back to the ice model. This melt field is then used as the melt rate in equation (3), and the ice thickness is advanced a single timestep, treating melt rates as fixed over that timestep. The ice model timestep is adaptive due to Courant-Friedrichs-Lewy (CFL) constraints, but is generally 0.1 years. It is the ice model timestep that is the actual coupled timestep in this framework; the integration of the ocean model is a spinup, and the melt rate field at the end of this spinup period is applied over a coupled timestep to the ice model. It is noted that *Grosfeld and Sandhager* [2004] used a coupling timestep of 50 years; however, their cavity was intended to be representative of that under the Filchner Ice Shelf, which has a longer timescale than those of the smaller ice shelves in the Amundsen Sea [*Jenkins et al.*, 1997; *Little et al.*, 2008], which are a closer analog to those used in the modeling conducted here.

[24] It is important to realize that, since coupling is asynchronous and the ice is isothermal, the only field in the coupled model with memory is the ice thickness. The rationale for our approach is as follows. We found in our preliminary investigations that the adjustment time of the melt rate field in cavities under small shelves with high thermal forcing is short relative to a characteristic ice model timestep (i.e., the one dictated by the CFL criterion). See section 5 for further discussion on this subject.

2.4. Experimental Procedure

[25] This paper details the results of a single coupled simulation using the model described above. As mentioned above, the temperature and salinity specified in the restoring region has a strong influence on ocean circulation within the ice shelf cavity, and so we expect the results of this simulation to depend strongly on these conditions. Five layers are

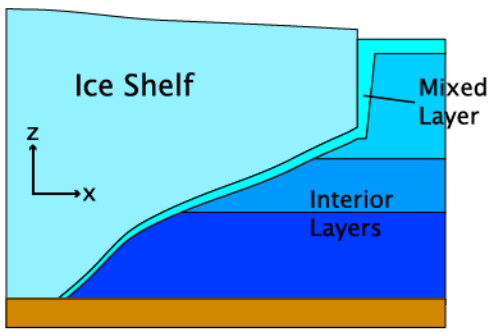

Figure 2. Schematic of longitudinal cross section of ocean cavity, indicating the mixed layer and ocean interior.

Table 2. Sponge (and Initial) Layer Temperatures, Salinities, and Thicknesses

Layer	Temp. (°C)	Salinity (psu)	Upper Interface Elevation
1	−1.9	33.0	0 m below surface
2	−1.9	33.1	5 m below surface
3	−1.8	34.0	10 m below surface
4	−0.6	34.21	−300 m
5	0.6	34.57	−700 m

used in the ocean model: a variable-density mixed layer and buffer layer, and three interior isopycnal layers. The profile is meant to capture the key aspects of water on the Amundsen Shelf: the upper layers are cold and fresh due to wintertime convection [*Assmann et al.*, 2005], while the layers at depth are generated by mixing with Circumpolar Deep Water. The details of the stratification are in Table 2.

[26] *Goldberg et al.* [2012] compares results of experiments with differing restoring conditions and differing grounded ice parameters. In that study we consider bottom temperatures between 0°C and 1.8°. Our particular experimental setup (i.e., with a bottom temperature of 0.6°C) was chosen to present in detail because it is within the middle of the range of stratifications investigated, and because it displays behavior common to all the experiments. We stress that, in making this choice, we are not making a statement about ocean conditions under any specific ice shelf.

[27] The experimental procedure is as follows. The ice model is time-integrated, without melting, to a steady state. This steady state is summarized by Figure 3, which shows ice velocities and grounding line position. Due to the shape of the bedrock, there is grounding at the margins of the ice shelf, and the shelf has an embayed shape (which is reminiscent of PIG, the bed profile of which inspired our analytically defined bed). Flow is predominantly in the positive x-direction (which can be expected from the boundary conditions), but there is some lateral convergence near the grounding line and lateral spreading near the front. This constitutes the initial state of the coupled experiment. The coupled model is then time-integrated according to the steps described in section 2.3 until the coupled system reaches what is considered to be a steady state (the exact meaning we use for "steady state" is explained in section 3). The experimental procedure described here is very similar to that of *Little et al.* [2012], which subject a stream-shelf system in equilibrium to a step change in melt rate parameters.

[28] Note that the initial melt-free steady state ice profile, along with constancy of ocean restoring conditions, essentially constitutes a very large step change in far-field ocean conditions (This is not a precise statement; it would be difficult to specify a stratification that would lead to no melting or freezing anywhere. But with sufficiently cool restoring conditions these melting and freezing rates would be small). In reality such changes would not be so large or so sudden. The magnitude of the perturbation was simply so that the response would be more pronounced and therefore easier to analyze. Our reasoning for the step change as opposed to, e.g., slowly "ramping up" far-field temperatures over a 10- or 20-year period, was to prevent any potential confusion of intrinsic timescales of the ice stream-ice shelf-ocean cavity system with imposed timescales of the forcing. The implications of these choices are discussed in the following section.

3. Results of Coupled Experiment

[29] The experiment is run for 250 years after melting is imposed, and a coupled steady state is achieved. This new state differs from the initial state of the model in all ice and ocean fields. However, as will be made clear below, the path to this coupled steady state involves multiple timescales on which the different components of the coupled system operate. And so rather than simply show the final state, the initial coupled adjustment of the ice shelf and melt field are presented first, followed by the grounded response, which occurs on a much longer timescale.

3.1. Coupled Adjustment of Ice Shelf and Melt Rates

[30] Since ice shelf geometry and melt rates influence each other strongly and on comparable timescales, they are discussed simultaneously. Melting leads to ice shelf thickness evolution both locally and nonlocally. The local thinning is through the last term on the right hand side of the continuity equation (3). The nonlocal effects are through advection by ice shelf velocity and dynamic thinning (thinning due to ice flow divergence). We observe that advection is the dominant of these effects over the initial ~10 years of adjustment. At the same time, modification of ice shelf thickness leads to changes in patterns and magnitudes of melt rates. Dynamic thinning (or rather changes in dynamic thinning rates) is important as well, but on a longer timescale, and so is discussed later.

[31] The changes in melt rate and ice shelf geometry over the first decade can be seen in Figure 4. This figure shows several fields relevant to the coupled response: ice shelf basal elevation, ice shelf basal slope magnitude (i.e., $\sqrt{b_x^2 + b_y^2}$), mixed layer velocity, mixed layer thickness, and melt rate. The effect of the ice shelf shape on circulation is

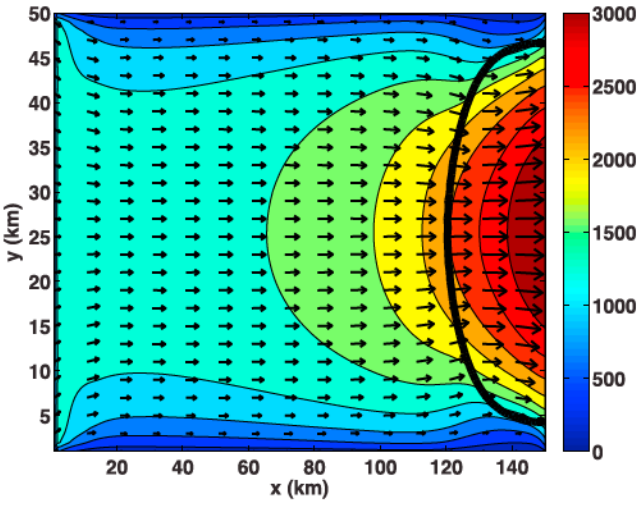

Figure 3. Initial state of the ice model in the coupled experiment. Vectors show ice velocity, and filled contours are magnitude of x-velocity, both in ma^{-1}. The thick black contour represents the grounding line.

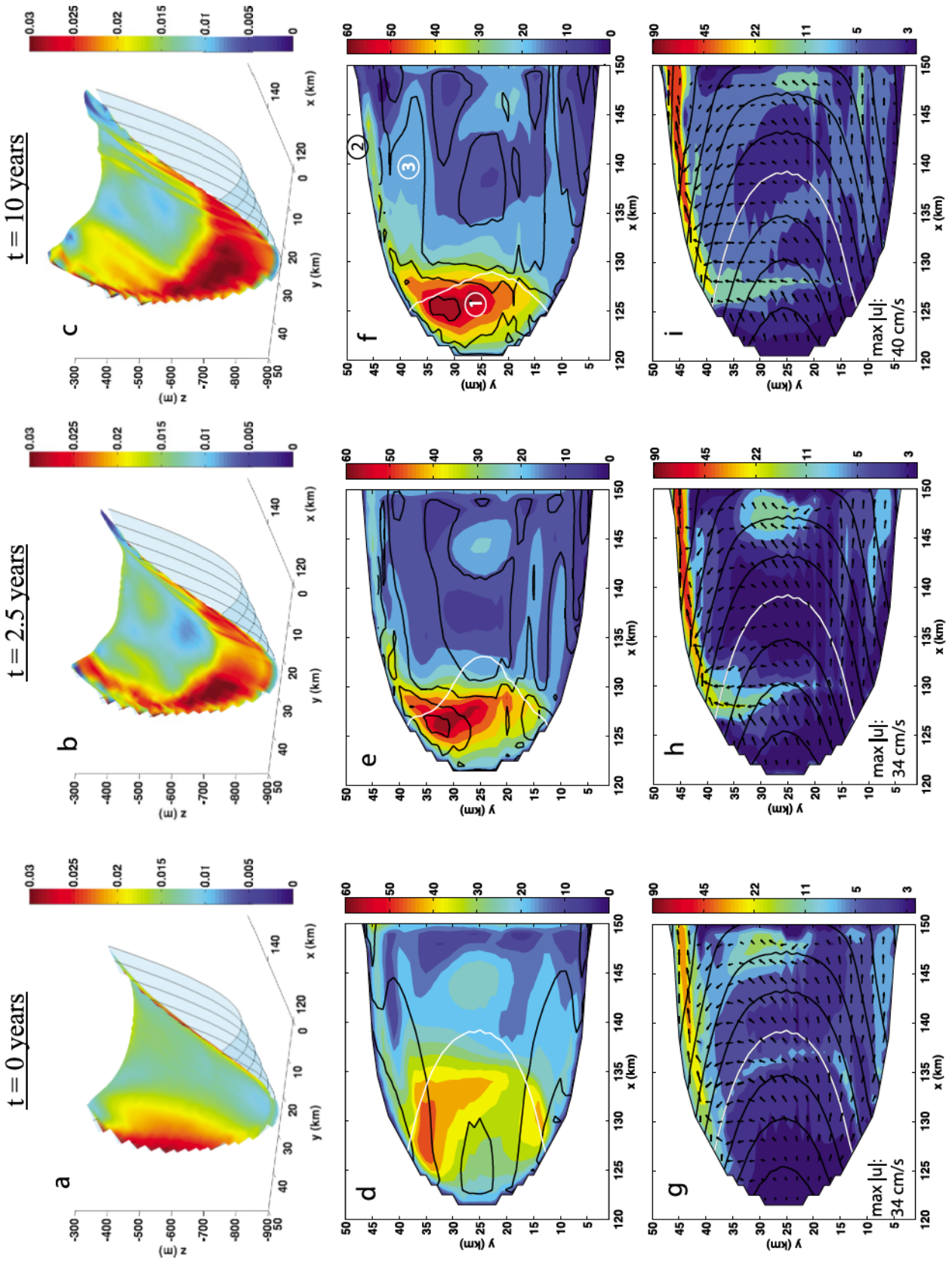
t = 0 years
t = 2.5 years
t = 10 years
a
b
c
d
e
f
g
h
i
z (m)
y (km)
x (km)
max |u|:
34 cm/s
40 cm/s
1
2
3

Figure 4

evident. The mixed layer flows in a direction slightly to the left of that of steepest ascent; this is a result of the balance between the buoyancy-induced pressure gradient, bottom friction, and Coriolis force. The angle of deflection from steepest-ascent increases with mixed layer thickness, as the layer-integrated Coriolis force scales with thickness but friction does not. The Coriolis effect leads to an asymmetric melt field, as well as convergence of the mixed layer along the left-hand margin (i.e., the "Coriolis-favored" side in the Southern Hemisphere) of the ice shelf, despite the initial symmetry of the ice shelf cavity. The resulting boundary current can have speeds on the order of 30 cm/s in our simulations.

[32] The pattern of melt rates is strongly controlled by ice shelf geometry. *Lane-Serff* [1995] describes two sub-ice shelf (ocean) dynamic regimes: one in which the mixed layer is relatively thin, and the heat balance is controlled primarily by the local effects of entrainment and melting; and one in which the mixed layer is thicker and advective effects become important. In these simulations, mixed layers are thin (less than 10m) in the interior of the cavity. Here, basal slope influences melt rates through its effect on velocity and turbulent entrainment of interior water. The thicker regime is evident only in the boundary-trapped outflow current, where there is strong horizontal flow convergence. In the boundary current, mixed layer temperature and melt rates are less sensitive to local geometry [*Little et al.*, 2009]. Additionally, ice shelf draft and ocean stratification control the melt pattern by determining the properties of the entrained water. It can be seen from the initial state that the highest melt rates occur in regions of elevated basal slope. However, high melt rates also correlate strongly with the presence of warm bottom water below ~700 m, which is the mean elevation of the upper interface of the warmest layer of interior water.

[33] The evolution of the coupled ocean-ice shelf cavity in the first decade of the experiment can be discussed in terms of three separate regions: the upstream-most 10 km of the ice shelf, referred to below as the "high-slope" region; the boundary current region; and the downstream region on the Coriolis-favored side of the shelf outside of the boundary current, referred to below as the "left-flank" region (these regions are numbered 1, 2, and 3, respectively, in Figure 4f). Each undergoes change, but in response to different controlling factors. Examining the system after only 2.5 years have passed (center column of Figure 4) reveals the shortest timescale of ice shelf response. By this time, the ice shelf has responded locally to melting near the grounding line, and basal slope has increased in the high-slope region (the slope increase can also be seen in Figure 7a). At the same time, the melt rate field has changed dramatically. Its maximum value has increased, along with the local ice shelf basal slope, and the region of high melt has been compressed longitudinally and is almost entirely within the high-slope region. The mixed layer circulation has changed in response to ice shelf geometry; there is now significant steering of the flow into the boundary current along the edge of the high-slope region. There is also an increase in mixed layer depth in the boundary current, due in part to this transport. Still, there has been relatively little downstream change in ice geometry, apart from that caused by local melting in the boundary current, which has led to the formation of a narrow channel.

[34] The pattern of ice shelf thinning in the first 2.5 years is shown more clearly in Figure 5a. Though thinning is significant elsewhere, it is clearly weighted toward the high-slope region. It is important to note that this thinning is not effected by the melt rate field shown in the Figure 4e; the melt rate evolves along with ice shelf thickness, and the thinning shown is the integrated effect of the evolving melt field and ice shelf dynamics. The thinning signal at the grounding line is carried downstream by advection, but since ice shelf velocities are ~2 km/year this has not had time to affect the ice shelf strongly.

[35] The rightmost column in Figure 4 shows the state of the system after 10 years of coupled simulation. Over the latter portion of the first decade, the changes are most obvious in the downstream regions, while ice geometry and melt rates in the high-slope region have changed relatively little. A tongue of elevated melt rates has developed in the left-flank region, coincident with an area of elevated basal slope. The development of this elevated melt/slope region involves close interaction between ice advection and melting. In this interaction a thinning differential set up by the transverse gradient in upstream melt rates is propagated downstream by ice advection, giving rise to an increased transverse slope. At the same time, the elevated longitudinal slope signal is advected as well. The melt rate responds to the change in slope, further accentuating the thinning. Additionally, the boundary current has widened, and its maximum speed has increased; it is not clear whether this is in response to increased flux from the left-flank region or from further upstream. Broadening of the channel in the boundary current region may also play a role in the current's width and depth.

[36] In Figure 5b we show thinning from 2.5 years to 10 years. That is,

$$h(t = 2.5 \text{ years}) - h(t = 10 \text{ years}),$$

such that thinning is positive, is shown. The thinning over this period is strongly downstream-weighted, with relatively little change in the high-slope, upstream region. One of the areas of greatest thinning is in the left-flank region (though thinning is still substantial in other downstream areas); this is in part due to the elevated melting in the left-flank region, coupled with ice advection.

Figure 4. Ice shelf, melt rate, and mixed layer properties at initial time (left), 2.5 years (middle), and 10 years (right). (a–c) Elevation (meters) and basal slope norm ($|\nabla b|$). The point of view is from upstream. The base of the cavity is indicated by a transparent surface. (d–f) Melt rates (shading, ma^{-1}) and basal slope norm (black contours). (g–i) Mixed layer depth (shading, meters; note the log scale), basal elevation (black contours) and mixed layer flow direction (vectors). Maximum mixed-layer speed (which occurs in the boundary current) is indicated in plots. In the first and second rows, the 700 m depth contour is indicated in white. Figure 4f shows the three regions discussed in the text: high-slope (1), boundary current (2) and left-flank (3). In Figures 4e and 4f basal slope contours are not shown in the boundary current region because they obscure view of melt rates.

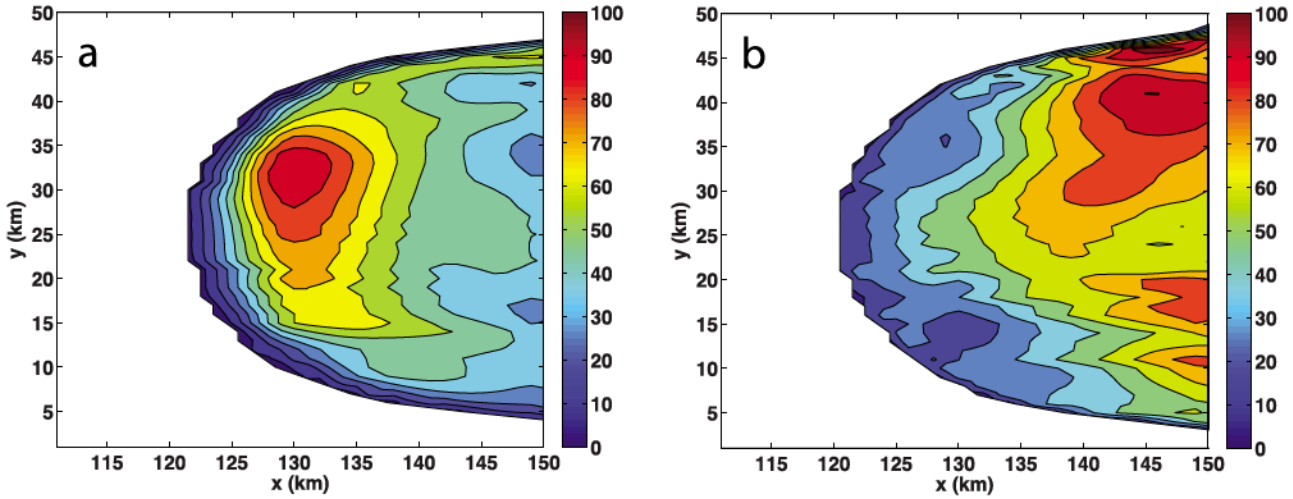

Figure 5. Ice shelf thinning (in meters) over the first decade of the 0.6°C experiment. Thinning is positive where thickness change is negative. (a) The thinning in the first 2.5 years. Note positive thinning implies a negative change in thickness. (b) The additional thickness change over period from 2.5 to 10 years.

[37] From Figures 4 and 5, two distinct timescales of coupled adjustment emerge. In the high-slope, upstream region ice geometry responds immediately to the onset of melting. Thinning and basal slope increase is eventually slowed by a corresponding increase of longitudinal advection. This is because further thinning without grounding line retreat would increase the basal slope and cause a thickening tendency due to advection. In other words, thinning is arrested when the local slope of the ice shelf base is increased to the point where

$$-\Delta(uh_x) \sim \dot{m} \tag{6}$$

in the region where the ice shelf is exposed to the warm water. Here $\Delta(uh_x)$ is the change in longitudinal advection, negative when there is a thickening tendency. The change is due mostly to changes in h_x, rather than u.

[38] On the decadal timescale, the initial thinning is carried downstream. The process is complicated, with advection, dynamic thinning, and the response of melt rates to adjusting shelf geometry contributing to thickness changes. The assertion that this is a decadal process, and not a longer one, is not obvious here. But in the next subsection we show that there is a shift in the main mode of change, from ice shelf-melt rate adjustment to grounded response, and this begins approximately a decade into the experiment.

[39] A question arises as to whether the fast timescale of slope adjustment near the grounding line is entirely due to the mean stratification. The stepwise nature of the stratification is an artifact of the 5-layer isopycnal discretization, and may give rise to the strong cutoff in melt rates. However, *Little et al.* [2012], who used a submarine melt rate parameterization dependent solely on ice shelf basal slope, showed similar rapid adjustment near the grounding line. Additionally, the strong separation of timescales could be in part due to the initial step change in ocean forcing: if the change in restoring conditions were continuous over e.g., a decade, the adjustment of the high-slope region could potentially overlap with that of the downstream region. Clearly, more experimentation is required to assess the role of the background temperature profile and its temporal forcing in setting the timescale of adjustment, and this is a subject of ongoing investigation.

[40] In Figures 4e and 4f, features in melt rate and transverse basal slope that are oriented with the direction of ice flow can be seen in the bottom-right. We attribute these features to small transverse features that already exist in ice thickness, orginating either in the ice stream or as a result of discretization of the floatation condition, which induce small variations in mixed layer speed and hence melt rates. The melt rate variations magnify the thickness variations slightly, whereas in an ice-only model the variations would not become noticeable. The variations in thickness and melt rates do not grow unstably (see Figure 10a), and melt rates remain larger in the boundary current and left-flank regions. Furthermore, it is likely that in a real ice shelf, small-scale thickness variations would be present in the ice stream as it flows across the grounding line, which would likely influence melt rate variations. In other words, the features arise from numerical artifacts, but we believe their growth and persistence may be physical.

3.2. Grounded Ice Response

[41] Throughout the early stages of model integration, flow in the longitudinal direction is ~2.4–2.5 km/year at the grounding line and ~3.1–3.5 km/year at the ice shelf front (where variations are larger due to the greater degree of thinning). However, this small variation, particularly at the grounding line, results in a mass imbalance that leads to marked changes in the ice stream interior. It has long been suggested, on theoretical [*Thomas*, 1979], modeling [*Schmeltz et al.*, 2002; *Dupont and Alley*, 2005; *Goldberg et al.*, 2009], and observational [*Krabill et al.*, 2000; *Shepherd et al.*, 2004; *Joughin et al.*, 2004; *Scambos et al.*, 2004] grounds that the thinning of floating ice shelves is related to speedup of grounded ice and subsequent grounding line retreat. Ice shelves in embayments can modify and moderate the stress field felt by grounded ice, and changes in the

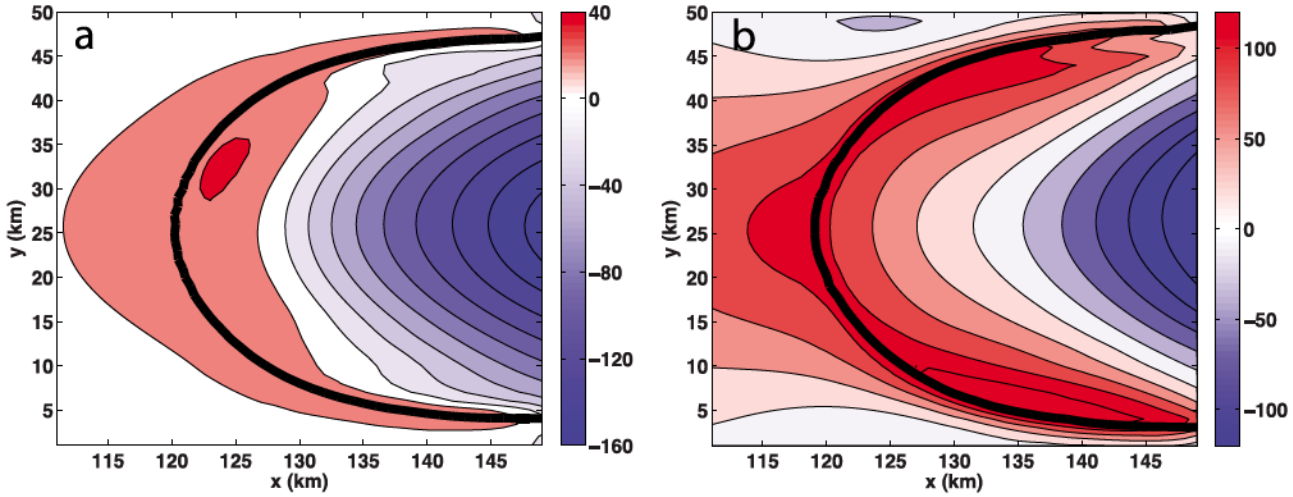

Figure 6. Anomaly in x-velocity (ma^{-1}) in the ice shelf and downstream part of the ice stream after initiation of melting. (a) Change after 2.5 years. (b) Additional change from 2.5 to 10 years. The thick black line denotes the grounding line. Note the differing color scales.

shelves' geometry (i.e., their thickness and spatial extent) can affect their ability to do so. The effects of this stress modification on the velocity field, the grounding line, and the grounded mass budget can be observed in our experiment, as shown below.

[42] As the ice shelf thins, the velocity within the shelf and at the grounding line changes. Figure 6a shows the change in x-velocity compared to the initial field. Ice has sped up at the grounding line, consistent with the idea that thinning of a shelf limits its ability to moderate longitudinal stress. Toward the center of the shelf front, however, the shelf has slowed. This is also consistent with theory, though; extensive stresses, and thus velocity gradients, increase with ice shelf thickness, especially in unconfined parts of the shelf, and so a thinner shelf would be expected to move more slowly (this can be seen quite clearly in a one-dimensional balance [e.g., *Van der Veen*, 1999]). The additional change during the period from 2.5 to 10 years (Figure 6b) has a larger magnitude but similar pattern; however, there is a somewhat amplified increase along the flanks of the grounding line. This could be connected to the concentration of thinning over this period on the side parts of the shelf. But velocity is related to shelf thickness in a very complicated way, so it can be misleading to draw meaning from such correlations.

[43] Beginning after ~10 years, a period of grounding line retreat is observed. This retreat arises because the velocity increase leads to thinning at the grounding line, thinning ice there to the point where it meets the floatation condition. At this point it becomes problematic to compare velocity fields

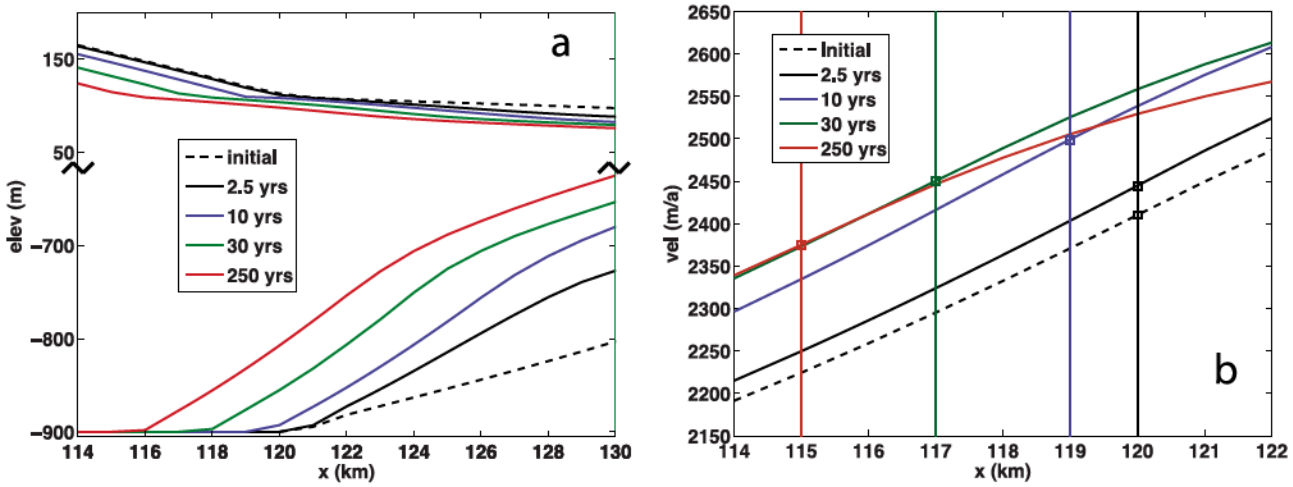

Figure 7. (a) Profiles (upper and lower surfaces) of the ice stream along the center line (y = 25 km) at various times. Note that the vertical scale is collapsed in order to show detail in both surface and basal profiles. (b) Corresponding center line velocity profiles at same time levels. Vertical lines indicate grounding line positions, and square markers indicate out grounding line velocities. All curves corresponding to a given time level are similarly colored.

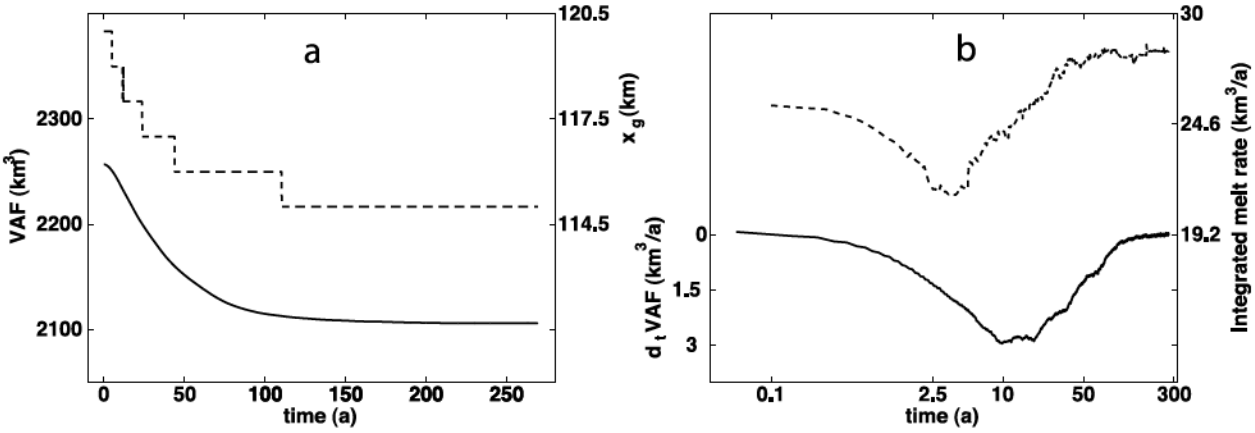

Figure 8. Transient evolution in 0.6°C experiment. (a) Volume above Floatation (*VAF*, solid) and minimum grounding line position (x_g, dashed). (b) *VAF* loss rate ($\frac{d(VAF)}{dt}$, solid) and spatially integrated melt rate (dashed). Note the logarithmic scale of the time axis.

as shown in Figure 6. We show the movement of the grounding line, together with thickness changes and velocities at the grounding line, in Figure 7. Over the course of the experiment, the grounding line recedes ~5 km. The first 10 years sees an increase of velocity at the grounding line of ~100 m/yr (which is only about 4–5% of the initial velocity). This is then followed by a slow decrease until the system reaches a steady state at ~250 years. The retreat and slowdown (or "recovery", as it is referred to below) is skewed toward earlier times; the 30-year time level is included to show this. Finally, note that, at the end of the experiment, the grounding line velocity has returned to a value close to its initial value.

[44] A time series can better give a feel for the timescales relevant to grounded response. The longitudinal position of the grounding line at the center of the domain (which is also the farthest upstream point of the grounding line), is used as a proxy for grounding line position; this value is referred to as x_g. We also introduce the metric of Volume Above Floatation, or *VAF* [*Dupont and Alley*, 2005], and defined by

$$VAF = \int_G \left[h - \left(-\frac{\rho_w}{\rho_i} R(x,y) \right)_+ \right] dA. \tag{7}$$

Here, integration is over the grounded portion of the domain (G), and the "+" subscript indicates only the positive part. One can see from (1) that changes to the ice shelf alone do not affect *VAF*. Rather, it is the volume of grounded ice in the domain such that, if it were to melt, would contribute to sea level rise. As such, it (and its rate of change) is a relevant and useful metric to quantify the overall effect of the ocean on a marine ice sheet. Figure 8a displays x_g and *VAF* as a function of time for the coupled experiment. Note that, although the x_g curve is discrete due to a cellwise-constant diagnosing of the floatation condition, the two trajectories are very similar. (The grounding line is considered to be on cell boundaries for diagnostic and plotting purposes only; while there is no explicit sub-grid tracking of the grounding line, the ice model uses a regularization of basal stress in partially grounded cells [*Goldberg et al.*, 2009].) The absolute value of *VAF*, however, is not as important as its change.

[45] Figure 8b shows the time rate of change of *VAF*. Here, the reason for the focus on the first 10 years of the experiment becomes clear: the first decade sees a sharp increase in the rate of loss of *VAF*, from approximately zero to 3 km^3/yr (in steady state, the loss rate of *VAF* should be zero). The loss is associated with increased velocities, and hence mass fluxes, across the grounding line. After 10 years the loss rate (defined here as a positive quantity) abruptly stops increasing, and then begins to decrease. We refer to this as "recovery" because the system is recovering from the shock of a sudden melting increase. Eventually, the flux imbalance is negligible, and the grounded domain approaches a new steady state.

[46] Also shown in Figure 8b is integrated melt rate, for comparison with the grounded mass imbalance. After melting is imposed at the beginning of the experiment, there is a drop in integrated melting over the first 2.5 years. This is nonintuitive, since the peak melt rate under the ice shelf increases over this period. However, it can be explained by a longitudinal compression of the region of high melting: though the maximum melt rate increases, the decrease in area exposed to the warmest water overcompensates, resulting in less overall melting. Integrated melt then increases again as melt rates rise in the left-flank region and the boundary current widens. Shelf extension contributes to an increase in integrated melt rate as well, but on a much longer timescale; on the decadal timescale it is the downshelf adjustment of melt rates that dominates the increase.

[47] As mentioned previously, the use of a no-melting state as an initial condition is arguably artificial. However, an additional experiment was done in which we perturbed a different coupled steady state, one in which ocean temperatures were cooler and melt rates were smaller (but still significant). The transient behavior and steady state were very similar to that of the experiment detailed above though of course the thinning rates were smaller in magnitude.

[48] Bed geometry plays a role in setting the timescale of grounding line movement. Grounding line retreat would be slowed over a bed that shallowed inland, and accelerated over a bed that deepened inland. In the extreme case, the retreat timescale could overlap with the shelf adjustment. The potential for merging timescales should be kept in mind

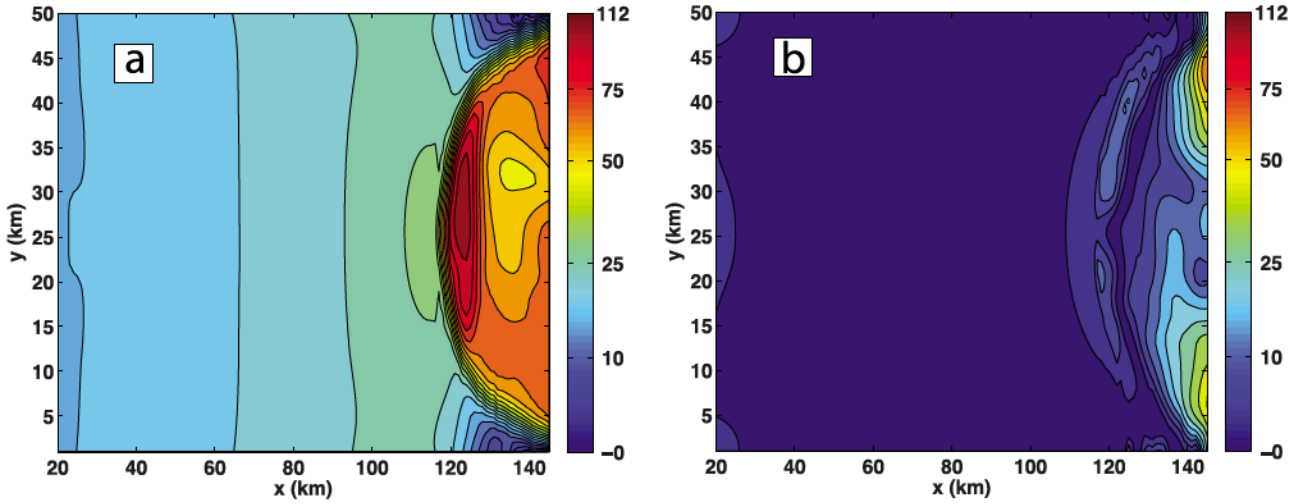

Figure 9. Total thinning (in meters) for the whole domain in the 0.6°C experiment subsequent to the first decade. Thinning is positive where thickness change is negative. Note the logarithmic scales. (a) Thinning over the period 10–250 years. (b) Thickness loss after shifting initial thickness profile by grounding line retreat distance, again over the 10–250 year period.

when attempting to apply the results in this section to realistic ice shelves.

4. Discussion

4.1. Long-Term Ice Shelf and Melt Rate Evolution

[49] The ice shelf-ocean response discussed above suggests multiple intrinsic timescales of response for the coupled system. There is a timescale of ~2–3 years when the region near the grounding line responds to the melting perturbation, and a decadal timescale over which changes in the shelf thickness and basal melt field are seen downstream, and velocities increase at the grounding line. There is also timescale on the order of centuries on which grounding line retreat occurs. Eventually, the grounding line retreat leads to its own termination through buttressing, as discussed in section 4.2.

[50] This separation of timescales of ice shelf change and grounded ice change can be further seen in overall thinning rates during this period of grounded ice adjustment. Figure 9a shows total thinning over the period from the end of the first decade to the end of the experiment, i.e.,

$$\Delta h = h(t = 250) - h(t = 10). \tag{8}$$

The region shown includes both the shelf and the upstream interior of the ice stream. Thinning is seen throughout the domain and is considerable (~20 m) as far as 100 km upstream from the grounding line. However, aside from the most downstream portions of the shelf, much of this thinning can be explained by the "translation" of the ice stream/ice

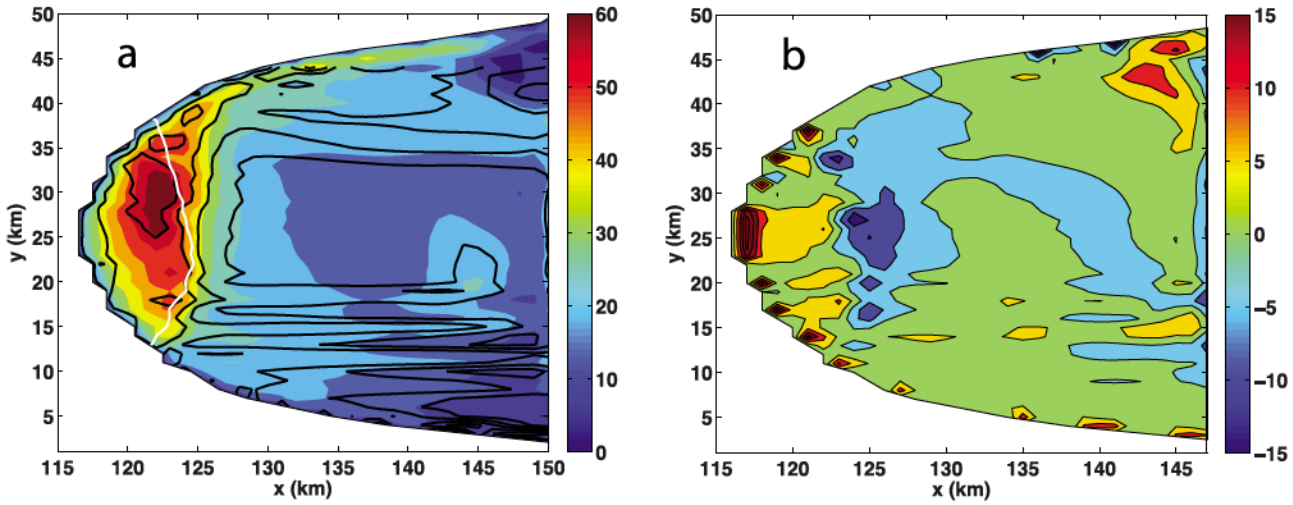

Figure 10. (a) Basal melt rate (filled contours, ma^{-1}), ice shelf basal slope (black contours) and 700 m depth contour (white) after 250 years of coupled integration. (b) Comparison with melt rate at 10 years, shifted left 3 km.

shelf system upstream with the retreat of the grounding line. That is, viewed from a frame that moves in the x-direction at the grounding line retreat rate, ice thickness changes are much smaller than those implied by Figure 9a. This is shown by Figure 9b, which plots

$$\Delta_{+4}h = h(t = 250, x) - h(t = 10, x + 4). \quad (9)$$

Note the colorscale is identical with Figure 9a. Here, the thickness changes are much smaller except for regions near the ice shelf front to either side of the shelf. This demonstrates that, as the grounding line retreats in our model, the grounded domain and a large part of the shelf adjust to maintain a characteristic shape relative to the grounding line.

[51] This concept also pertains to the melt rate: Figure 10a displays melt rate and slope after 250 years. A comparison with the melt rate field at 10 years shows similarities, both in shape and magnitude, of with respect to melt rates in the high-slope, left-flank, and boundary current regions. In Figure 10b we compare melt rates at $t = 10$ years and $t = 250$ years, translating as in (9), and this reveals a relatively small anomaly. However, the horizontal shift in this case was 3 km, not 4 km; that is, the melt rate field has been translated ~3 km upstream over the course of the retreat. This is likely because ice in the first floating grid cell has not thinned significantly in the final steady state, as can be seen in Figure 7a.

[52] This constancy of the melt rate field relative to the grounding line is in part due to the bed geometry; we would not expect a similar result if the bed deepened inland, due to the strong role played by the mean stratification. But the result does mean that the lengthening of the ice shelf at the expense of grounded ice does not have a strong control on the upstream geometry. Thus, in the final stage of adjustment, the grounded ice change, as well as much of the change in the coupled shelf cavity-ocean system, is due to grounding line movement and large-scale bed geometry (It is possible that external changes, such as sea level rise and grounded flow variability, can manifest on the century timescale. However, the effects of such changes are beyond the scope of this study).

4.2. Importance and Nature of Buttressing

[53] The ability of an ice shelf to transmit resistive stresses from its margins to the high-fluxing regions of its grounding line, otherwise known as ice shelf buttressing, is a well-known phenomenon. But rarely has its effect on grounded ice change been connected to specific changes in ice shelf morphology. In section 3, we showed similarities between broad patterns in ice shelf change and grounded ice response. Specifically, before large grounding line movement can occur, large amounts of thinning must occur in the shelf; thinning, without changes in ice shelf extent, leads to increased grounding line velocities and eventual loss of grounded ice volume. Once grounding line retreat occurs, the ice shelf becomes longer (since the ice front is fixed), which has a marked effect on mass flux across the grounding line.

[54] *Little et al.* [2012] suggests that, under parameter regimes similar to the ones in this study, the relative changes in shelf thickness and length are more important to buttressing than changes in ice shelf velocity during adjustment to increased melting. Thus buttressing is approximately proportional to the "side area" of the shelf over which lateral drag is present. Although the authors used a parameterization for buttressing, and "side area" is an ambiguous term in the current study considering the three-dimensionality of the ice shelf, the concept is still useful in the interpretation of the grounded ice response. During the initial stage of coupled adjustment of ice shelf and melt rates, the ice shelf thins without extension, and at the same time the rate of loss of grounded ice volume increases. A turning point occurs at the end of this stage, and the effects of shelf lengthening are seen. From this point on the grounded response is dominated by the effect of shelf lengthening (note our distinction between the role of velocity change in buttressing, which is relatively small, and its role in grounded ice volume balance, which is important).

[55] In the coupled steady state reached at the end of the simulation, flux across the grounding line is in balance with flux input at the upstream boundary, just as in the initial state. The upstream flux input is constant in time, meaning grounded flux has returned to its initial level (with any imbalance being negligible relative to the early decades of the experiment). As seen from Figure 7, velocity at the center of the grounding line is close to its initial value.

[56] It is reasonable to expect that resistive stress has returned to initial levels as well. While this may not be intuitive, we offer this rationalization: a long literature of theoretical and modeling studies [e.g., *Weertman*, 1974; *Thomas*, 1977; *Thomas and Bentley*, 1978; *Schoof*, 2007a; *Nowicki and Wingham*, 2007; *Durand et al.*, 2009] supports the idea that ice flux at the grounding line is related to longitudinal stress. In particular, the analysis of *Schoof* [2007a] suggests that for a given grounding line depth, basal traction, and ice stiffness parameter, ice flux is proportional to normal stress at the grounding line. As bed depth does not change in the along-flow direction, we can then expect that the amount of resistive stress needed to achieve a given flux will remain the same.

[57] Given this assumption, we can then rationalize the new steady state: the initial thinning of the shelf reduces its ability to transfer resistive stress. As the grounding line retreats, its basic geometry (modulo translation, cf. Figure 9b) remains constant over much of its extent. Thus, the shelf needs to be longer to provide the same buttressing as it did in its initial, thicker, uncoupled steady state.

[58] We note that the above discussion is heuristic, making use of a number of constructs developed for discussing flowline models of marine ice sheets. A full analysis of the stress balance and its relation to the grounded mass balance and shelf geometry would be beyond the scope of this exploratory study. We defer such a discussion to a separate study.

4.3. Propagation of Thinning and Timing of Retreat

[59] In section 3.1, advection of the thinning and slope increase at the grounding line was cited as the reason for a melting increase in the left-flank region subsequent to the development of the high-slope region. The role of advection is highlighted by Figure 11, which is a Hovmöller diagram of longitudinal basal slope, as well as change in ice thickness, along the longitudinal transect $y = 40$ km over the first 15 years of integration. Along a slope contour, $\frac{\partial b}{\partial x}$ (where

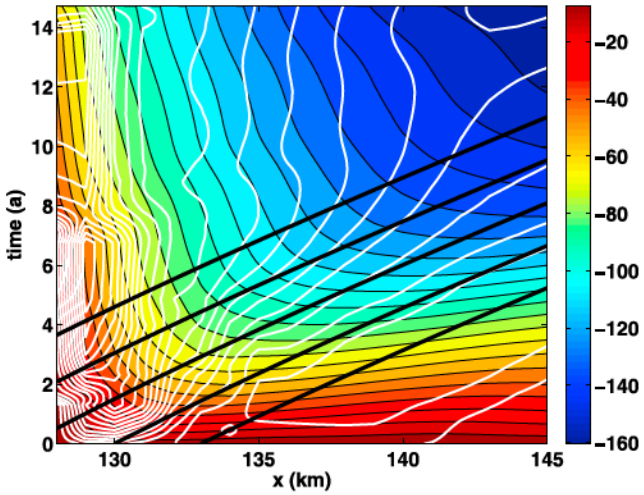

Figure 11. Hovmöller diagram, showing thinning (in meters) and slope as a function of x and t along the longitudinal transect $y = 40$ km. Filled contours represent ice shelf thickness change from the beginning of experiment. White curves are contours of constant longitudinal basal slope ($\frac{\partial b}{\partial x}$). Thick black lines represent particle trajectories in the ice shelf.

$b(x, y)$ is basal elevation) is constant. Slope contours coincide strongly with Lagrangian trajectories leaving the region ~130–135 km (the downstream end of the high-slope region) after 1–2 years. The evolution of transverse slope, not shown due to its complexity, does not show such a clear pattern of longitudinal advection. Still, as mentioned earlier, longitudinal slope along explains a nonnegligible portion of the slope magnitude throughout the left-flank region.

[60] Thickness is continually decreasing due to melting, so we do not expect contours of thickness change to coincide with Lagrangian trajectories. However, the contours become more vertically oriented after Lagrangian trajectories originating from near the grounding line pass through them. This implies an end to the fast (decadal) adjustment of ice shelf thickness [see also *Little et al.*, 2012, Figure 4e]. This illustrates that, while local melt-induced thinning downstream plays a role in the adjustment of the shelf, advection from upstream is a key component as well. This is confirmed by the trajectory of *VAF* loss rates. The loss rate reaches a maximum after about 10 years and then begins to decrease, indicating an end to the fast-timescale thinning that, up to that point, has been able to counter the shelf extension due to retreat.

[61] It was mentioned previously that the imposition of a step change in ocean forcing is somewhat artificial, and may be at least partly responsible for the clear separation between upstream and downstream adjustment timescales in the ice shelf. But given the importance of ice shelf advection to downstream adjustment, as well as the upstream-weighted melt rates observed in our experiments, the lagged component of the downstream ice shelf response may be a robust characteristic of adjustment to warming ocean temperatures. However, further experimentation would be needed to assess this claim.

[62] Note the behavior shown in Figure 11 depends on a separation of timescales between the processes of shelf advection and grounding line retreat, which to some extent depend on the model setup. As mentioned earlier, a foredeepened bed geometry could lead to faster grounding line retreat. The dependence of the advective timescale on model parameters is explored further in *Goldberg et al.* [2012].

5. Caveats

[63] Our study is largely exploratory in nature; knowledge of land ice-ocean interactions is relatively limited and we seek to learn about basic behaviors. At the same time, it is important that the assumptions and limitations inherent in our model be clearly stated. This allows not only for the degree of applicability of model results to be assessed, and the identification of processes that are not included, but may be relevant to ice-ocean coupling in general.

5.1. Coupling Methodology

[64] A drawback of our coupling procedure is that, in each coupled timestep, the ocean model is started from an unrealistic flat-isopycnal state. An alternative would be restarting the model from its state at the end of the previous coupled timestep. However, such an approach is problematic for the following reasons. In our coupled framework, the nature of our model components is such that the ice model cannot be updated too frequently because the time required for the nonlinear ice velocity solver and the transfer of data between the models would become impractically large. Thus, when the ocean model is started as part of a coupled timestep (see section 2.3), it sees an imposed surface pressure field that is very different from that of the previous coupled timestep (shelf thickness changes over an ice model timestep can be on the order of tens of meters, translating to several bars). Additionally, it potentially sees a new domain, due to the floatation or grounding of cells (i.e., "wetting" and "drying" of ocean cells, respectively). Simply restarting the ocean model from its state at the end of the previous coupled timestep leads to large (and artificial) barotropic waves that lead to persistent, artificially large melt rates.

[65] Owing to these difficulties, we take the approach of starting the ocean model from a flat-isopycnal state: while this also leads to barotropic adjustment during spinup, it avoids the issue of zero-thickness columns (essentially a wetting-and-drying problem) and is programatically easier to implement.

[66] Similarly, other details of the setup are guided by the computational need to minimize the spinup time required for the ocean model at each coupled timestep (with a 1-km ocean model, the computational requirements to integrate the ocean model for a combined time of several centuries are considerable, even with a relatively small domain). The ice shelf front is smoothed numerically, as a sharp spatial change in surface pressure, from ice shelf overburden to atmospheric, is observed to prolong the time needed for spinup (This smoothing is only for the purposes of coupling and is not seen by the ice model. The smoothed portion extends into the restoring region, and is not shown in any of the figures in this manuscript). Additionally, the restoring was made quite strong in order to minimize the effect of strong barotropic waves resulting from an imposition of a surface pressure field at every coupled timestep. The effect of doubling the restoring time constant was assessed. It was

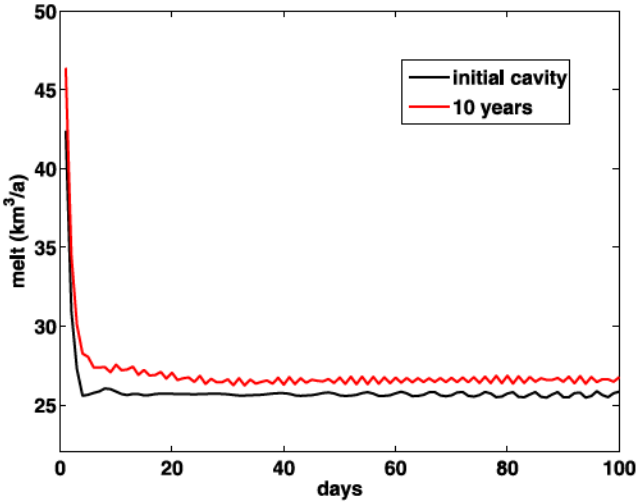

Figure 12. Area-integrated melt rate as a function of time for fixed cavity geometries. The geometries considered are that of the initial cavity, and that of the coupled model 10 years after the initial melt perturbation. Values are daily averages.

seen that it took longer for the melt rate field to steady, but once it did the differences were minimal, and largely confined to downstream areas of the shelf near the center of the front.

[67] The ocean spinup time in all of our simulations was 15 days. This time period was chosen based on preliminary assessment with the ocean model, over a range of restoring parameters and restoring temperatures. However, cavity geometries arising from coupled interaction were not considered in this assessment: we chose the spinup time based on the behavior of the ocean model alone. A posteriori examination suggests that a slightly longer spinup time may have been optimal. Figure 12 shows daily averages of area-integrated melt rates for two fixed cavity geometries: that of the initial cavity, and the one generated by 10 years of coupled integration. Both use the same restoring time constants as in the coupled experiment. 15 days is seen to be sufficient for the initial geometry (recall that the trailing 5-day average is used for coupling). For the 10-year geometry, while much of the adjustment takes place within the initial 15-day period, it seems a spinup of ~25 days would have been more appropriate. We note, however, that the variations in total melt rate after the initial 15-day period are small compared to the overall variations in melt rate over the course of the coupled simulation, and we do not expect that a longer spinup time would qualitatively change the results of the experiment. Furthermore, the spinup time required does not lengthen after the initial decadal coupled adjustment.

5.2. Treatment of Open Ocean

[68] In our ocean model setup, the entire open ocean section was restored, i.e., there was no unforced open ocean. While this likely had little effect on melt rates near the grounding line, open ocean treatment could affect circulation in the outflowing boundary current.

[69] In other simulations with our coupled model, which are detailed in *Goldberg et al.* [2012], an anticyclonic circulation developed in the mixed layer that guided the relatively warm outflow slightly away from the ice shelf margin. For several isolated timesteps, an unforced section of open ocean was placed between the calving front and the restoring, and it was observed that this circulation strengthened relative to the case of no unforced open ocean. This does not necessarily take away from the results of the study; rather, it highlights the fact that open-ocean processes near the ice shelf front (e.g., sea ice formation, wind stress) may strongly influence the overall behavior of the coupled system.

[70] It should be mentioned that the problems with our approach described in this subsection and the last arose from "fixes" that were deemed necessary for the particular setup used in this study. They are by no means fundamental roadblocks to simulating ice-ocean interactions. All that is required is tighter integration of the codes of the two models, which is planned for the near future.

5.3. Ice Shelf Thermodynamics

[71] The ice model in our study is isothermal. As such, the Glen's Law coefficient A is spatially constant, and the basal heat flux into the ice interior, which is proportional to the basal ice temperature gradient, is parameterized assuming a column is in thermal steady state, as in *Holland and Jenkins* [1999]. In an ice shelf, diffusion of heat into the interior can potentially have an effect on its internal temperature, affecting both the basal temperature gradient and the stiffness of the ice shelf, so it is important to consider the implications of the isothermal assumption. In all of our simulations, the basal melt rate was positive, and considerably large over most of the shelf. It can be shown using scaling arguments that the thermal boundary layer, the depth of the ice shelf over which the effects of melting are felt, is on the order of tens of centimeters for our simulations, and adjusts on the order of hours. Additionally, the short residence time of the ice shelf (on the order of a decade) further prevents thermal effects at the base from being felt in the interior.

[72] Thus, for small, strongly thermally forced (i.e., "warm") ice shelves, we expect that feedback of basal heat flux into the shelf on either ice flow or basal melt rates is a higher-order effect. The same likely cannot be said of "cold" ice shelves, where the water entering the shelf cavity at depth has been cooled to near-surface temperatures, and melt rates are an order of magnitude smaller.

[73] Note we are not suggesting that temperature variations within ice shelves are unimportant; on the contrary, the effect of temperature on the flow dynamics of ice shelves has been shown to be an important one [*Larour et al.*, 2004, 2005]. Rather we are stating that in the case of a "warm" ice shelf, heat uptake from the ocean does not affect internal temperatures, nor does it feed back on melt rates.

5.4. Ice Shelf Calving and Shear Margin Strength

[74] The calving front was held fixed in all of the simulations in this study, which prevented any examination of calving effects on the dynamics. This is important because shelf lengthening, and implicitly the stationary calving front, played a large role in the system eventually finding a coupled steady state. There is no agreed-upon universal calving law for ice shelves [*Benn et al.*, 2007], but one could also

expect that thinning of a shelf might lead to retreat of the calving front.

[75] Of equal importance to ice shelf stress balance is ice rigidity. It has long been thought that shear margins are softer than the interior of an ice stream or ice shelf, due to strain heating and intense crevassing [*Echelmeyer et al.*, 1994]. Studies of ice shelf rheology support this [*Larour et al.*, 2005]. It may be that margins would effectively soften as a greater burden is placed on them, magnifying the effect of margin thinning. With these considerations in mind, the grounded response in our simulations may serve as a lower bound.

6. Conclusions

[76] In this study a three-dimensional ocean model was thermodynamically and geometrically coupled to a dynamic ice stream-ice shelf model capable of representing grounding line migration, in such a way that the ocean model could influence the ice model through basal melting and the ice model could affect the ocean model through thickness and surface pressure. The model is novel in that both its ice and ocean components are dynamic, transverse variation is resolved, and grounding line migration is possible. A coupled experiment was conducted, which involved exposing an ice stream-ice shelf system that was in steady state to a sudden change in far-field ocean conditions, and observing the response in the melt rate field, the ice shelf geometry, and the evolution of grounded ice. The ocean conditions corresponded to the "warm" ocean conditions of the type observed near the Amundsen Sea ice shelves.

[77] The experiment showed a distinct pattern of adjustment, spanning multiple timescales. The ice shelf was seen to adjust on the decadal scale, initially thinning and steepening near the grounding line, then thinning further downstream due to melting in a rotationally induced ocean boundary current as well as due to advection of upstream thinning. The melt rate field, controlled strongly by ice shelf geometry as well as background stratification, changed considerably over this time, becoming both more concentrated near the grounding line and developing higher melt rates within and near the outflowing boundary current. The modification of the ice shelf geometry led to grounded ice thinning and grounding line retreat through stress field modification. This stress imbalance was eventually offset, on a much longer timescale, by ice shelf lengthening (due to grounding line retreat with a fixed calving front). In the process described above, the maximum rate of retreat was reached after a decade, corresponding to the timescale of adjustment due to ice shelf advection. This suggests the important role that ice shelf advection plays in the response to melting.

[78] *Little et al.* [2012], who used a flowline model and a parameterized melt rate dependent on along-flow basal slope, saw the same separation of timescales, as well as a similar pattern of quick retreat followed by slow recovery. It is possible that the response observed in this study could be reproduced using a similar basal slope-based parameterization, perhaps augmented by a depth-dependence to reflect an imposed stratification. However, such an approach would neglect certain aspects of the circulation, such as the high melt rates in the mixed layer boundary current, which may be of importance in the grounded ice response.

[79] Conclusions of this study are presented with a cautionary note due to limitations of our coupled framework, and should be verified in other studies. Nevertheless, we believe that the multiple intrinsic timescales and their clear separation in adjustment of the ice stream-ice shelf-ocean system to instantaneous thermal perturbation are robust results, which will be useful for further investigations of land ice-ocean interaction.

[80] **Acknowledgments.** D.N.G. received funds from the Princeton AOS Postdoctoral and Visiting Scientist Program, and from NSF award ANT-1103375. C.M.L. received funds from the Princeton Carbon Mitigation Initiative. D.N.G. and C.M.L. received funds from the STEP program in the Woodrow Wilson School of Public and International Affairs, Princeton University. O.V.S. received funds from NSF awards ANT-0838811 and ARC-0934534. Stephen Price, Eric Larour, one anonymous reviewer, and editors Poul Christofferson and Bryn Hubbard contributed helpful comments to the manuscript. D. M. Holland and K. S. Smith kindly provided additional CPU time.

References

Assmann, K. M., H. Hellmer, and S. S. Jacobs (2005), Amundsen Sea ice production and transport, *J. Geophys. Res.*, *110*, C12013, doi:10.1029/2004JC002797.

Benn, D. I., C. R. Warren, and R. H. Mottram (2007), Calving processes and the dynamics of calving glaciers, *Earth Sci. Rev.*, *82*, 143–179.

Determann, J., M. Thoma, K. Grosfeld, and S. Massmann (2012), Impact of ice-shelf basal melting on inland ice-sheet thickness: A model study, *Ann. Glaciol.*, *53*(60), 129–135, doi:10.3189/2012AoG60A170.

Dupont, T. K., and R. Alley (2005), Assessment of the importance of ice-shelf buttressing to ice-sheet flow, *Geophys. Res. Lett.*, *32*, L04503, doi:10.1029/2004GL022024.

Durand, G., O. Gagliardini, B. de Fleurian, T. Zwinger, and E. Le Meur (2009), Marine ice sheet dynamics: Hysteresis and neutral equilibrium, *J. Geophys. Res.*, *114*, F03009, doi:10.1029/2008JF001170.

Echelmeyer, K. A., W. D. Harrison, C. Larsen, and J. E. Mitchell (1994), The role of the margins in the dynamics of an active ice stream, *J. Glaciol.*, *40*, 527–538.

Goldberg, D. N., D. M. Holland, and C. G. Schoof (2009), Grounding line movement and ice shelf buttressing in marine ice sheets, *J. Geophys. Res.*, *114*, F04026, doi:10.1029/2008JF001227.

Goldberg, D. N., C. M. Little, O. V. Sergienko, A. Gnanadesikan, R. Hallberg, and M. Oppenheimer (2012), Investigation of land ice-ocean interaction with a fully coupled ice-ocean model: 2. Sensitivity to external forcings, *J. Geophys. Res.*, *117*, F02038, doi:10.1029/2011JF002247.

Grosfeld, K., and H. Sandhager (2004), The evolution of a coupled ice shelf-ocean system under different climate states, *Global Planet. Change*, *42*, 107–132.

Grosfeld, K., R. Gerdes, and J. Determann (1997), Thermohaline circulation and interaction between ice shelf cavities and the adjacent open ocean, *J. Geophys. Res.*, *102*, 15,595–15,610.

Hallberg, R., and A. Gnanadesikan (2006), The role of eddies in determining the structure and response of the wind-driven southern hemisphere overturning: Results from the modeling eddies in the southern ocean (meso) project, *J. Phys. Ocean.*, *36*, 2232–2252.

Heimbach, P., and M. Losch (2012), Adjoint sensitivities of sub-ice shelf melt rates to ocean circulation under Pine Island Ice Shelf, West Antarctica, *Ann. Glaciol.*, *54*, 59–69, doi:10.3189/2012/AoG60A025.

Hindmarsh, R. C. A. (2006), The role of membrane-like stresses in determining the stability and sensitivity of the antarctic ice sheets: Back pressure and grounding line motion, *Philos. Trans. R. Soc. A*, *364*, 1733–1767.

Holland, D. M., and A. Jenkins (1999), Modelling thermodynamic ice-ocean interactions at the base of an ice shelf, *J. Phys. Ocean.*, *29*, 1787–1800.

Holland, D. M., S. S. Jacobs, and A. Jenkins (2003), Modelling the ocean circulation beneath the Ross Ice Shelf, *Antarct. Sci.*, *15*, 13–23.

Holland, P. R., A. Jenkins, and D. M. Holland (2008), The response of ice shelf basal melting to variations in ocean temperature, *J. Clim.*, *21*, 2558–2572.

Jacobs, S. S., A. F. Amos, and P. M. Bruchhausen (1970), Ross sea oceanography and antarctic bottom water formation, *Deep Sea Res. Oceanogr. Abstr.*, *17*(6), 935–962, doi:10.1016/0011-7471(70)90046-X.

Jacobs, S. S., A. Jenkins, C. Giulivi, and P. Dutrieux (2011), Stronger ocean circulation and increased melting under Pine Island Glacier ice shelf, *Nat. Geosci.*, *4*, 519–523, doi:10.1038/NGEO1188.

Jenkins, A. (1991), A one-dimensional model of ice shelf-ocean interaction, *J. Geophys. Res.*, *96*, 20,671–20,677, doi:10.1029/91JC01842.

Jenkins, A. (1999), The impact of melting ice on ocean waters, *J. Phys. Ocean.*, *29*, 2370–2381.

Jenkins, A., and D. M. Holland (2002), A model study of ocean circulation beneath filchner-ronne ice shelf, Antarctica: Implications for bottom water formation, *Geophys. Res. Lett.*, *29*(8), 1193, doi:10.1029/2001GL014589.

Jenkins, A., D. G. Vaughan, S. S. Jacobs, H. H. Hellmer, and J. R. Keys (1997), Glaciological and oceanographic evidence of high melt rates beneath Pine Island Glacier, West Antarctica, *J. Glaciol.*, *43*(143), 114–121.

Jenkins, A., P. Dutrieux, S. S. Jacobs, S. D. McPhail, J. R. Perrett, A. T. Webb, and D. White (2010), Observations beneath Pine Island Glacier in West Antarctica and implications for its retreat, *Nat. Geosci.*, *3*, 468–472, doi:10.1038/ngeo890.

Joughin, I., and R. B. Alley (2011), Stability of the West Antarctic ice sheet in a warming world, *Nat. Geosci*, *4*, 506–513, doi:10.1038/ngeo1194.

Joughin, I., W. Abdalati, and M. Fahnestock (2004), Large fluctuations in speed on Greenland's Jakobshavn Isbrae glacier, *Nature*, *432*, 608–610.

Joughin, I., B. Smith, and D. M. Holland (2010), Sensitivity of 21st century sea level to ocean-induced thinning of Pine Island Glacier, Antarctica, *Geophys. Res. Lett.*, *37*, L20502, doi:10.1029/2010GL044819.

Krabill, W., et al. (2000), Greenland ice sheet: High-elevation balance and peripheral thinning, *Science*, *289*, 428–430.

Lane-Serff, G. F. (1995), On meltwater under ice shelves, *J. Geophys. Res.*, *100*, 6961–6965.

Larour, E., E. Rignot, and D. Aubry (2004), Processes involved in the propagation of rifts near Hemmen Ice Rise, Ronne Ice Shelf, Antarctica, *J. Glaciol.*, *50*(170), 329–341, doi:10.3189/172756504781829837.

Larour, E., E. Rignot, I. Joughin, and D. Aubry (2005), Rheology of the Ronne Ice Shelf, Antarctica, inferred from satellite radar interferometry data using an inverse control method, *Geophys. Res. Lett.*, *32*, L05503, doi:10.1029/2004GL021693.

Little, C. M., A. Gnanadesikan, and R. Hallberg (2008), Large-scale oceanographic constraints on the distribution of melting and freezing under ice shelves, *J. Phys. Ocean.*, *38*, 2242–2255.

Little, C. M., A. Gnanadesikan, and M. Oppenheimer (2009), How ice shelf morphology controls basal melting, *J. Geophys. Res.*, *114*, C12007, doi:10.1029/2008JC005197.

Little, C. M., et al. (2007), Toward a new generation of ice sheet models, *EOS Trans. AGU*, *88*, 578–579.

Little, C. M., D. N. Goldberg, A. Gnanadesikan, and M. Oppenheimer (2012), On the coupled response to ice-shelf basal melting, *J. Glaciol.*, *58*, 203–215.

MacAyeal, D. R. (1989), Large-scale ice flow over a viscous basal sediment: Theory and application to Ice Stream B, Antarctica, *J. Geophys. Res.*, *94*, 4071–4087, doi:10.1029/JB094iB04p04071.

Nicholls, K. W., S. Osterhus, K. Makinson, T. Gammelsrød, and E. Fahrbach (2009), Ice-ocean processes over the continental shelf of the southern Weddell Sea, Antarctica: A review, *Rev. Geophys.*, *47*, RG3003, doi:10.1029/2007RG000250.

Nowicki, S. M. J., and D. J. Wingham (2007), Conditions for a steady ice sheet-ice shelf junction, *Earth Planet. Sci. Lett.*, *265*, 246–255.

Parizek, B. R., and R. T. Walker (2010), Implications of initial conditions and ice–ocean coupling for grounding-line evolution, *Earth Planet. Sci. Lett.*, *300*(3–4), 351–358, doi:10.1016/j.epsl.2010.10.016.

Paterson, W. S. B. (2001), *The Physics of Glaciers*, 3rd ed., Butterworth-Heinemann, Oxford, U. K.

Payne, A. J., A. Vieli, A. Shepherd, D. J. Wingham, and E. Rignot (2004), Recent dramatic thinning of largest West Antarctic ice stream triggered by oceans, *Geophys. Res. Lett.*, *31*, L23401, doi:10.1029/2004GL021284.

Payne, A. J., P. R. Holland, A. Shepherd, I. C. Rutt, A. Jenkins, and I. Joughin (2007), Numerical modeling of ocean-ice interactions under Pine Island Bay's ice shelf, *J. Geophys. Res.*, *112*, C10019, doi:10.1029/2006JC003733.

Pollard, D., and R. M. DeConto (2009), Modelling West Antarctic Ice Sheet growth and collapse through the past five million years, *Nature*, *458*, 329–332.

Rignot, E., D. G. Vaughan, M. Schmeltz, T. K. Dupont, and D. R. MacAyeal (2002), Acceleration of Pine Island and Thwaites Glaciers, West Antarctica, *Ann. Glaciol.*, *34*, 189–194.

Scambos, T., J. A. Bohlander, C. A. Shuman, and P. Skvarca (2004), Glacier acceleration and thinning after ice shelf collapse in the Larsen B embayment, Antarctica, *Geophys. Res. Lett.*, *31*, L18402, doi:10.1029/2004GL020670.

Schmeltz, M., E. Rignot, T. K. Dupont, and D. R. MacAyeal (2002), Sensitivity of Pine Island Glacier, West Antarctica, to changes in ice-shelf and basal conditions: A model study, *J. Glaciol.*, *48*, 552–558.

Schoof, C. (2007a), Marine ice sheet dynamics. Part I. The case of rapid sliding, *J. Fluid Mech.*, *573*, 27–55.

Schoof, C. (2007b), Ice sheet grounding line dynamics: Steady states, stability, and hysteresis, *J. Geophys. Res.*, *112*, F03S28, doi:10.1029/2006JF000664.

Shepherd, A., and D. J. Wingham (2007), Recent sea-level contributions of the Antarctic and Greenland ice sheets, *Science*, *315*, 1529–1532.

Shepherd, A., D. J. Wingham, and J. Mansley (2002), Inland thinning of the Amundsen Sea sector, West Antarctica, *Geophys. Res. Lett.*, *29*(10), 1364, doi:10.1029/2001GL014183.

Shepherd, A., D. J. Wingham, and E. Rignot (2004), Warm ocean is eroding West Antarctic Ice Sheet, *Geophys. Res. Lett.*, *31*, L23402, doi:10.1029/2004GL021106.

Thomas, R. H. (1977), Calving bay dynamics and ice-sheet retreat up the St. Lawrence Valley System, *Geogr. Phys. Quat.*, *31*, 347–356.

Thomas, R. H. (1979), The dynamics of marine ice sheets, *J. Glaciol.*, *31*, 347–356.

Thomas, R. H., and C. R. Bentley (1978), A model for the Holocene retreat of the West Antarctic Ice Sheet, *Quat. Res.*, *10*, 150–170.

Van der Veen, C. J. (1999), *Fundamentals of Glacier Dynamics*, Balkema, Rotterdam, Netherlands.

Walker, R. T., and D. M. Holland (2007), A two-dimensional coupled model for ice shelf-ocean interaction, *Ocean Modell.*, *17*, 123–139.

Weertman, J. (1957), Deformation of floating ice shelves, *J. Glaciol.*, *3*, 38–42.

Weertman, J. (1974), Stability of the junction of an ice sheet and an ice shelf, *J. Glaciol.*, *13*, 3–11.